ELSEVIER

Earth and Planetary Science Letters 199 (2002) 185–200

EPSL

www.elsevier.com/locate/epsl

Paleogeography of the Amazon craton at 1.2 Ga: early Grenvillian collision with the Llano segment of Laurentia

Eric Tohver [a,*], B.A. van der Pluijm [a], R. Van der Voo [a], G. Rizzotto [b], J.E. Scandolara [b]

[a] *Department of Geological Sciences, University of Michigan, Ann Arbor, MI 48109-1063, USA*
[b] *CPRM, Av. Lauro Sodré 2561, Porto Velho, RO, 78904-300 Brazil*

Received 17 December 2001; received in revised form 15 February 2002; accepted 25 February 2002

Abstract

A paleomagnetic, geochronologic and petrographic study was undertaken on the flat-lying gabbros and basalts of the Nova Floresta Formation of Rondônia state, western Brazil in order to constrain the Mesoproterozoic paleogeography of the Amazon craton. Measurement of the anisotropy of magnetic susceptibility on the gabbroic samples reveals a flat-lying foliation with a radiating pattern of lineations, supporting the field evidence that the gabbros are part of a large, undeformed sill. Petrographic observations of oxides in the gabbros reveals two populations of magnetite grains produced during the original cooling of the sill: large, oxyexsolved titanomagnetite grains and fine-grained magnetite in igneous reaction rims. New $^{40}Ar/^{39}Ar$ age dating of biotite and plagioclase yield ages of ~1.2 Ga, which represent the rapid cooling following emplacement of the mafic magma. Whole rock dating of basalt samples yields total gas ages of 1062 ± 3 Ma, similar to the ~1.0 Ga K/Ar ages reported by previous workers. However, the strong compositional dependence of the age spectrum renders this younger whole rock age unreliable except as a minimum constraint. A single magnetic component is found in the basalts, indistinguishable from the characteristic remanence found in the gabbros that is oriented WNW and steeply upward. This magnetization is considered to be primary and was acquired during the cooling of the sill and associated lavas. A paleomagnetic pole calculated from the Nova Floresta Formation ($n = 16$ sites, $P_{lat.} = 24.6°N$, $P_{long.} = 164.6°E$, $A_{95} = 5.5°$, $Q = 5$), the first reported pole for the Amazon craton for the 1200–600 Ma Rodinia time period, constrains the paleogeographic position of Amazonia at ~1.2 Ga. Juxtaposition of the western Amazon craton with the Llano segment of the Laurentia's Grenville margin causes the NF pole to lie on the 1.2 Ga portion of the combined APWP for Laurentia and Greenland, which indicates that a collision with the Amazon craton could have caused the Llano deformation in early Grenvillian times.

Keywords: Amazon Basin; paleomagnetism; Rondonia Brazil; Rodinia; Grenvillian orogeny; Laurentia; Llano Uplift

1. Introduction

Paleogeographic reconstructions for the Proterozoic have suggested a long-lived connection be-

* Corresponding author. Tel.: +1-734-647-2157; Fax: +1-734-763-4690.
E-mail address: etohver@umich.edu (E. Tohver).

0012-821X/02/$ – see front matter
PII: S0012-821X(02)00561-7

tween Laurentia and Amazonia, the largest cratonic areas of North and South America, respectively [1,2]. Recognition of the Grenville Province as the product of continent–continent collision led to the proposed juxtaposition of Grenville-aged mobile belts of the western Amazon craton (Sunsas-Aguapeí belts) with the Laurentian Grenville province. This collisional history marks the amalgamation of the Rodinia supercontinent at 1.2–1.0 Ga. Given the total length of the Neoproterozoic rifts that circumscribe the continent, Laurentia is considered to occupy a keystone position within the Rodinia supercontinent [3]. The breakup of the supercontinent along Laurentia's eastern margin is initiated with the opening of the Iapetus ocean at the very end of the Proterozoic. Marine sediments recording the opening of Iapetus are found in both eastern Laurentia [4] and western Amazonia [5].

Independent evidence for the involvement of several major cratons in the Rodinia supercontinent is provided by paleomagnetism. The main approach used involves the matching of 1.1–0.95 Ga Grenville-aged APWPs for Laurentia, Baltica, Congo-São Francisco, and the Kalahari cratons [6,7]. This analysis rotates APWPs of similar age and shape into alignment, producing a paleomagnetically constrained Rodinia configuration in large agreement with that of Hoffman [2]. One of the shortcomings of these constrained Rodinia reconstructions is the absence of a colliding continent with the southernmost extension of Laurentia, i.e. the Llano Uplift area of central Texas (e.g. [1,2,7]). Dalziel et al. [8] addressed this problem, citing paleomagnetic data for the post-collisional 1.1–1.0 Ga interval in support of the Kalahari as the continent involved. However, existing data demonstrate more than 1500 km of latitudinal separation between Laurentia and the Kalahari [8,9].

Grenville-aged metamorphism and deformation is known to have affected the entire 3500 km eastern margin of Laurentia stretching from Labrador to central Texas [10,11]. The complex nature and timing of tectonometamorphism varies substantially along strike, typically recording early episodes of arc accretion culminating in continent–continent collision. In general, peak deformation ages associated with the final episodes of collision young to the northeast along (present-day) orogenic strike. Following accretion of the 1.3 Ga Coal Creek arc complex in the Llano Uplift region, continent–continent collision is documented as having occurred between 1238 ± 8 Ma and 1119 ± 6 Ma [11–13]. Similarly, the Grenville belt of the Adirondacks region and southeastern Ontario records a polymetamorphic history with accretion of the Elzevir arc terrane (1350–1185 Ma) followed by peak deformation at 1090–1010 Ma associated with final continent–continent collision [14–19]. The youngest Grenville deformation ages are found in the Labrador region of Canada where evidence of an accretionary event is lacking [19]. Here the $\sim$990 Ma metamorphic ages unambiguously reflect deformation of Paleoproterozoic to Archean basement rocks [20] with post-tectonic granite intrusions occurring from 974 to 956 Ma [21].

Recent regional mapping undertaken by the Brazilian Geological Service (CPRM) has revealed the existence of large scale, strike-slip shear zones (Ji-Paraná shear zone (JPSZ) in Fig. 1) affecting the basement rocks of the Amazon craton [22]. Cooling from this amphibolite-grade deformation is recorded by hornblende $^{40}Ar/^{39}Ar$ ages which range from $\sim$1.18 to 1.15 Ga [23], coeval with collisional deformation recorded in the Llano Uplift. However, the lack of paleomagnetic data from Amazonia for this time period has prevented the meaningful evaluation of the proposed Laurentia–Amazonia connection within the Rodinia framework. The purpose of this paper is to establish a link between the early Grenvillian deformation of the western Amazon craton and deformation of the Grenville province of Laurentia.

2. Regional geology

The JPSZ is a strike-slip, sinistral shear zone that crosscuts the poylcyclic basement rocks of the western Amazon craton. Hornblende cooling ages from this early Grenville deformation range from 1.18 to 1.15 Ga [23]. Younger Grenville-aged deformation (ca. 1.0 Ga) is found in two metamorphic belts of the western Amazon region,

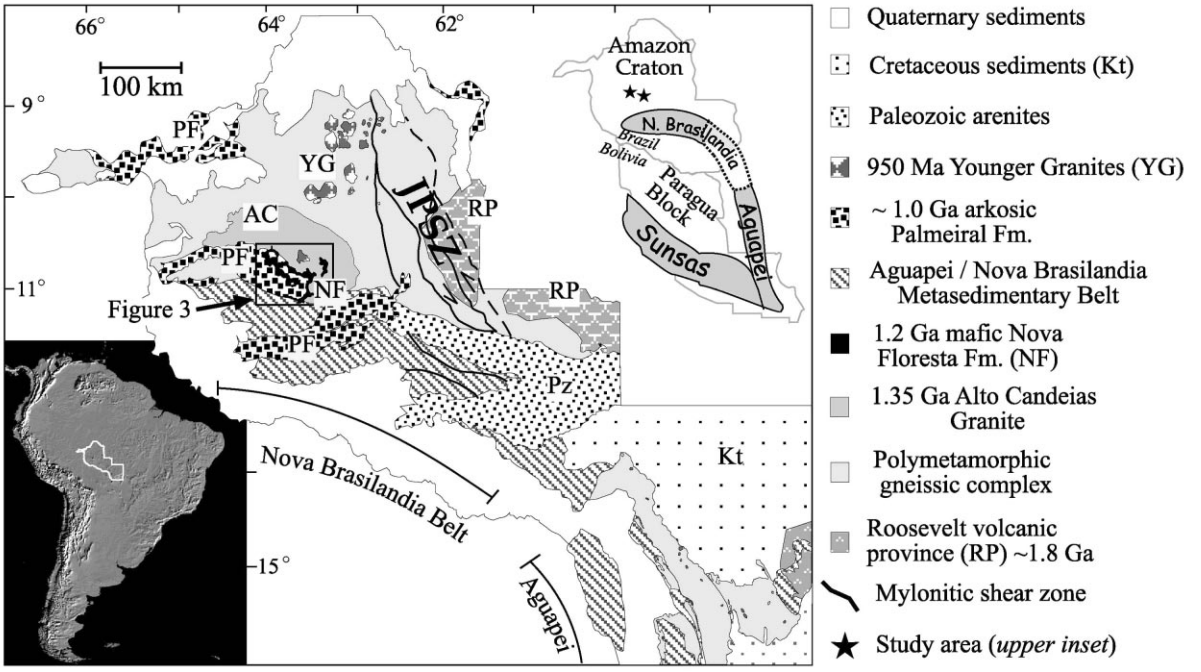

Fig. 1. Simplified geological map of the SW Amazon craton exposed in the Brazilian states of Rondônia and Mato Grosso adapted from [22]. Outlined area is depicted in more detail in Fig. 3. Bottom inset: South American location map. Top inset: sketch map of the Grenville-aged Sunsas and Aguapeí belts.

i.e. the Sunsas and Aguapeí belts exposed in Bolivia and Brazil, respectively [24]. Sandwiched between these two belts lies the Paragua craton, which preserves a ca. 2.0 Ga metamorphic basement intruded by the ~1.3 Ga Pensamiento batholith. Recent regional scale geological mapping undertaken by the CPRM, the Brazilian geological survey, in conjunction with new single mineral $^{40}Ar/^{39}Ar$ dating of basement samples, suggests that the Aguapeí belt and Nova Brasilândia belt to the northwest are part of the same monocyclic, metasedimentary belt deformed at ~1.0 Ga [22,23]. The younger ca. 1.0 Ga cooling history of this belt, together with the deep water nature of sediments in the Nova Brasilândia portion of belt, suggests that the Paragua craton may represent an exotic terrane accreted to the Amazon craton during late Grenvillian times (Fig. 1, top inset).

The mafic Nova Floresta Fm. (NFF) is found in isolated outcrops north of the Nova Brasilândia Metasedimentary Belt in Rondônia state, within the stable, undeformed portion of the Amazon craton proper. The hypabyssal microgabbros and sub-aerial, columnar basalts that comprise the NFF have a total thickness estimated at 300 m [25,26]. Outcrops of basalt display varying degrees of alteration and epidotization, while gabbros are commonly massive and unaltered. The NFF intrudes the 1346 ± 5 Ma Alto Candeias granitic suite (U/Pb zircon) [27]. The NFF is overlain by the flat-lying, crossbedded, pink arkoses of the Palmeiral Fm. (PF). Although no conclusive contact with the underlying NFF has been found, we consider the PF to be significantly younger than the NFF based on an angular unconformity between the PF and the ~1.0 Ga metasediments of the Nova Brasilândia Belt.

3. Sampling and methods

A total of 123 samples were collected from the basalts and gabbros of the NFF from 16 sites

distributed in two regions ~75 km apart, one located on the NE margin of the formation and the other sampling region located on the northern margin. Oriented samples were collected in the field with a gasoline-powered drill and a magnetic compass from fresh outcrops judged to be in situ. No discernible magnetic anomalies were observed. Site locations were recorded with a Garmin X12 GPS, which was also used to verify compass directions.

Measurement of the anisotropy of magnetic susceptibility (AMS) was carried out using a Geofyzika Brno KLY-2 Kappabridge instrument. Fifteen positions were measured on each of six samples per site. Eigenvectors representing the axes of the magnetic ellipsoid were calculated using procedures outlined by Jelinek [28]. An average of 12–16, standard 2.54-cm diameter specimens were demagnetized using either a Sapphire Instruments SI-4 AF demagnetizer (maximum field strength of 200 mT) or an Analytical Services Co. shielded oven. AF demagnetization was carried out in ~15 steps per specimen with 2–5 mT steps below 40 mT and 10–30 mT steps above 30 mT. Thermal demagnetization was carried out in 22 steps with 50° steps up to 400°, 25° steps from 400 to 500°C, and 5–10° steps from 500 to 580°C. Magnetic moments were measured after every step using a three-axis cryogenic 2G magnetometer in the field-free room at the University of Michigan. Remanence directions were calculated for all samples using principal component analysis [29] of linear demagnetization vectors picked from orthogonal projection plots [30]. An average of seven points per specimen was used to define a vector with a mean angular deviation of less than 8°.

Petrographic observations were made on polished thin sections using both a standard Leitz optical microscope and a Toshiba scanning electron microscope. Quantitative analysis of some phases was performed using a Cameca Camebax electron microprobe with a backscattered electron imager. Both natural and synthetic mineral phases were used as probe standards. All mineral phases were analyzed with wavelength dispersive PET, TAP, and LiF crystal spectrometers. Anhydrous phases were analyzed with a point beam (ca. 1 μm) using an accelerating voltage of 15 kV and a sample current of 10 nA.

Portions of the paleomagnetic drill core samples selected for $^{40}Ar/^{39}Ar$ geochronology were crushed, sieved, rinsed with deionized water and dried. Biotite and plagioclase grains ranging in size from 375 to 850 μm were picked by hand. Whole rock samples from the basalt were also prepared. Aluminum foil-packaged samples were irradiated for 10–14 days at the University of Michigan Ford Phoenix Reactor. Neutron fluxes were monitored with the 1071 ± 2 Ma 3gr standard [31]. Single grains were step-heated until fused using a defocused argon-ion laser to ensure uniform sample heating. Non-argon components were extracted using two 1/s SAES getters (ST101 alloy) and a liquid N_2 cold finger. Argon isotopic ratios were measured with a Mass Analyzer Products 215 mass spectrometer with a Niers source and Balzer electron multiplier. Extraction line blanks were run after every 10 heating steps. Duplicates were run on all samples to determine grain to grain variability and reproducibility of results. Plateau ages cited in the text reflect five or more consecutive steps representing > 50% of the total gas whose ages overlaps within error at the 2σ level. All argon isotopic data have been made available in the **Background Data Set**[1].

4. Results and observations

4.1. Petrography

The NFF comprises sub-alkaline to alkaline tholeiites with up to 2.0 wt% K [24]. Basalts are typically altered by hydrothermal activity with epidote and calcite infilling of amygdaloidal cavities. The plutonic equivalents of these rocks are predominantly olivine gabbros with minor anorthositic gabbros. Typical assemblages are plag+ol+aug+pig+ilm+mag+opx+bio ± kspar ± Fe-sulfides. Olivine ($Fo_{50}Fa_{50}$) is prismatic to rounded in form and is commonly rimmed by symplectitic intergrowths of orthopyroxene and magne-

[1] http://www.elsevier.com/locate/epsl

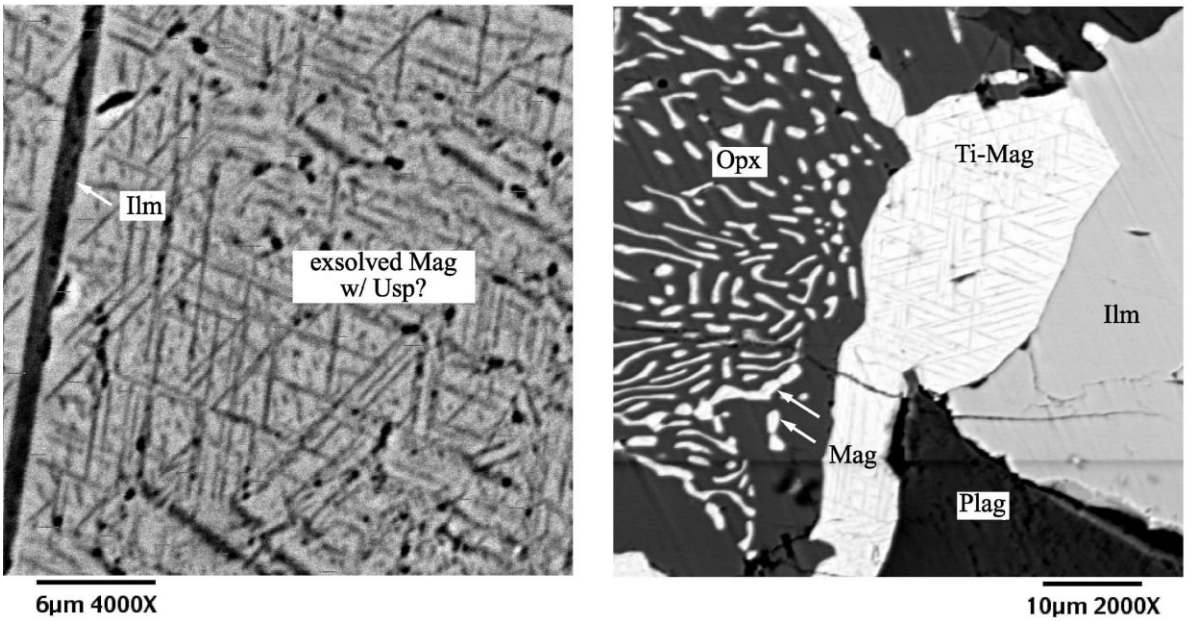

Fig. 2. (a) Oxyexsolution textures of magnetite+ilmenite ± ülvospinel found in large magmatic Ti-magnetites. (b) Small particles of magnetite found intergrown with orthopyroxene at reaction rims between olivine (not shown), magmatic magnetite (with oxyexsolution texture) and magmatic ilmenite.

tite, especially where in contact with magmatic ilmen ite. Plagioclase grains are elongate and columnar with slight zoning, displaying ophitic to sub-ophitic intergrowths with clinopyroxene ($En_{040.6}Fs_{15.8}Wo_{43.5}$) and orthopyroxene ($En_{57.7}Fs_{39.4}Wo_{2.9}$). Biotite occurs as a late magmatic phase, commonly rimming ilmenite.

Ilmenite and magnetite are the most common opaque minerals with minor abundances of pyrrhotite. Magnetite occurs in two distinct populations: as micron to sub-micron scale intergrowths with ilmenite in large, magmatic Ti-magnetite ($Mt_{0.82}Usp_{0.18}$) and in symplectitic intergrowths with orthopyroxene at grain boundaries between olivine and ilmenite (Fig. 2). The extremely fine-grained nature of both of these magnetite phases renders accurate microprobe analysis difficult, given the matrix interference that compounds the problem of evaluating ferric iron content by stoichiometry.

Two observations based on these microanalyses are emphasized. First, a range of magnetite compositions can be found within the oxyexsolved magmatic Ti-magnetite (C2–C3 stage of Haggerty [32]) with a minimum variation from $Mt_{90.1}Usp_{9.9}$ to $Mt_{59.5}Usp_{40.5}$. This variation in magnetite composition would likely be responsible for a similar range in Curie temperatures for the individual magnetite sub-grains. Secondly, the presence of Ti in the symplectitic magnetite suggests that it is formed by an oxidation reaction of olivine+il-menite to form orthopyroxene+magnetite. Note that both magnetite populations are considered to have been produced during the original cooling of the magma due to deuteric alteration of once homogeneous Ti-magnetite and the development of igneous oxidation reaction rims. If this inference is true, the magnetic remanence carried by either magnetite population would be a high temperature chemical remagnetization, albeit one acquired early enough to be considered primary.

4.2. Magnetic fabric and paleomagnetism

The bulk susceptibility measurements of the gabbroic samples have high average values of $\sim 3 \times 10^{-2}$ SI, suggesting that the magnetic fabric

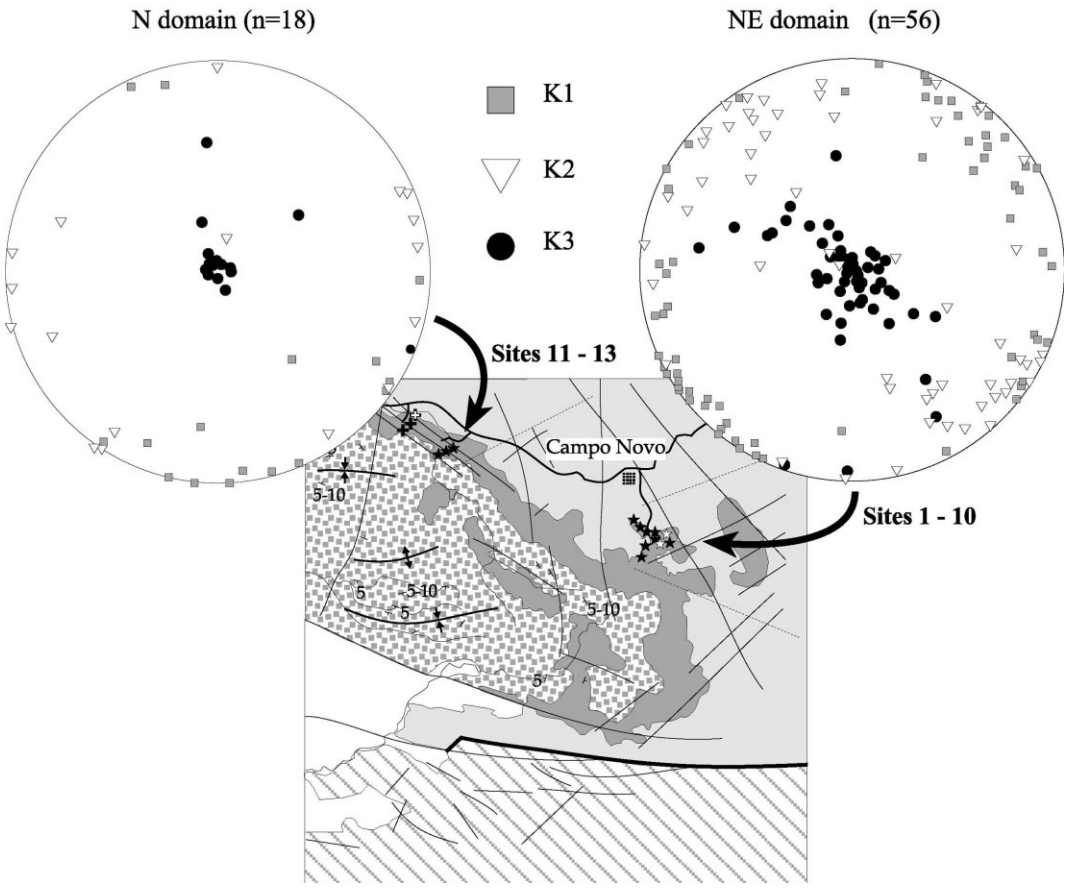

Fig. 3. Map: area outlined in Fig. 1 showing distribution of gabbro (★) and basalt (+) sample sites along NFF. Hollow symbols indicate sites used for $^{40}Ar/^{39}Ar$ dating. Inset stereonets: axes of AMS ellipsoid from the two sampling regions indicated by black arrows. Note the predominance of a flat-lying foliation and a radiating pattern of magnetic lineations, suggestive of emplacement from a central vent.

is dominated by the ferromagnetic contribution *sensu lato*. Values for the normalized degree of anisotropy, H, range from 0.011 to 0.105 with symmetrical distribution around the mean value of 0.048. Shape anisotropy is expressed as T, with oblate fabrics characterized by $0 < T \leq 1$ and prolate fabrics characterized by $-1 \leq T < 0$ [33]. Values for T range from -0.83 to 0.89, with most values clustering symmetrically around the mean value of 0.08, or slightly oblate. Both oblate and prolate anisotropies are common, even within the same site. A clear magnetic fabric present at all sites and in all samples is characterized by K_3 axes at steep angles corresponding to a horizontal magnetic foliation (Fig. 3). The distribution of K_1 axes varies with geographical distribution; sites located in the NE portion of the NFF are marked by NE-trending magnetic lineations whereas samples from the northern margin of the NFF are characterized by N-trending magnetic lineations.

Measurement of J/J_0 during thermal demagnetization demonstrates both steep- and soft-shouldered curves for both gabbros and basalts. There is no apparent correlation of demagnetization profile with lithology. All magnetic components are removed by 550–580°C, suggesting that Ti-poor magnetite is the principal carrier. Basalt samples are characterized by a single magnetic component whereas gabbro samples tend to dis-

Table 1
Location and demagnetization data for individual sites from the NFF

Site	Location (UTM)	n/N_{sp}	Dec.	Inc.	k	R	α_{95}
Gabbro sample sites:							
RON-01	20L 0436997 8818344	6/6	313	−58	24.5	5.8	13.8
RON-02[a]	20L 0433127 8818986	8/8	299	−61	76.2	7.91	6.4
RON-03	20L 04325542 8818480	6/8	309	−66	27.3	5.82	13.1
RON-04	20L 0436142 8818632	8/8	298	−55	98.6	7.93	5.6
RON-05	20L 0439158 8816988	8/8	297	−60	143.4	7.95	4.6
RON-06[b]	20L 0438717 8818110	6/8	296	−69	30	5.83	12.4
RON-07[b]	20L 0437746 8818028	8/8	299	−64	288.8	7.98	3.3
RON-08	20L 0436349 8818326	8/8	294	−67	63.3	7.71	7.6
RON-09	20L 0435359 8818383	8/8	281	−62	205	7.97	3.9
RON-10	20L 0431313 8818783	7/8	275	−69	55.8	6.89	8.1
RON-11	20L 393313 8836580	8/8	284	−67	173.1	7.96	4.2
RON-12	20L 0393340 883648	7/8	283	−71	36	6.83	10.2
RON-13	20L 0393635 8836327	8/8	288	−50	13.3	7.47	15.8
Mean direction from gabbro sites: $D = 295.1$, $I = -63.2$, $\alpha_{95} = 4.4$							
Basalt sample sites:							
RON-14[c,d]	20L 0387623 8837566	8/8	295	−53	66.4	7.89	6.8
RON-15[d]	20L 0387623 8837566	8/8	296	−40	14.7	7.59	16.3
RON-16[d]	20L 0387623 8837566	3/5	283	−50	8.9	2.78	44
Mean direction from basalt sample sites: $D = 291.5$, $I = -47.5$, $A_{95} = 12.3$							

[a] Specimen from site used for $^{40}Ar/^{39}Ar$ dating of plagioclase.
[b] Specimen from site used for $^{40}Ar/^{39}Ar$ dating of biotite.
[c] Specimen from site used for $^{40}Ar/^{39}Ar$ dating of whole rock.
[d] Actual drilling sites ±300 m due to interference from forest canopy.
Grand mean calculated from all 16 sites: $D = 294.2$, $I = -60.3$, $R = 15.76$, $k = 61.9$, $A_{95} = 4.7$

play a significant, secondary magnetic overprint. Both thermal and AF demagnetization revealed the single magnetic component for basalt samples oriented NW with steep, upward directions (Fig. 4a–f). AF demagnetization was used to isolate individual magnetic components in gabbroic samples (Fig. 4g–i); thermal demagnetization of gabbroic samples results in the simultaneous removal of two components (Fig. 4j–l). J/J_0 profiles for AF demagnetization depict the removal of up to 95% of the magnetic moment of most samples by 15–25 mT with a steeply up, NW ChRM isolated at fields >30 mT (Fig. 4g–i). This 'hard' component is similar to the ChRM isolated in the basalts, suggesting that both were acquired at about the same time (Table 1). The direction of the secondary overprint is not consistent between sites, i.e. distributed along many different great circles

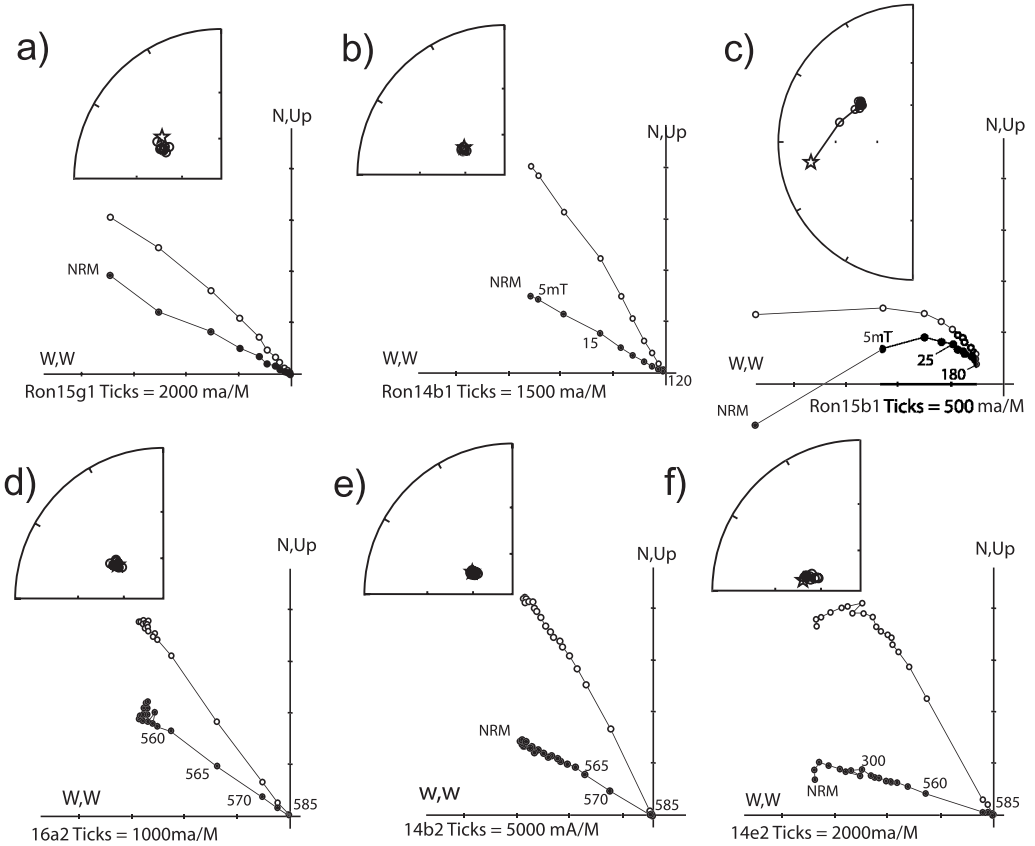

Fig. 4. Representative Zijderveld diagrams from AF demagnetization of basalts (a–c); thermal demagnetization of basalt (d–f); AF demagnetization of gabbro with insets showing removal of characteristic magnetic component proceeding to the origin (g–i); and thermal demagnetization of gabbro (j–l) samples. The *y*-axis is up and North for all plots.

with some samples recording NRMs antipodal to the ChRM. A paleomagnetic pole (24.6°N, 164.6°E, $A_{95} = 5.5$) was calculated from the virtual geomagnetic poles determined from individual site means.

4.3. Geochronology

Single grains of biotite from two different samples (from sites 6 and 7) display a very homogeneous distribution of radiogenic argon throughout the release spectrum. The total gas age for both of these samples, 1196 ± 2 to 1199 ± 3 Ma, agree within error and are similar to the respective plateau ages of 1198 ± 3 to 1201 ± 2 Ma (Fig. 5a,b). Measurement of the Ca/K ($^{37}Ar/^{39}Ar$) and Cl/K ($^{37}Ar/^{39}Ar$) ratios in both samples reveals a very homogeneous composition with no significant argon contribution from alteration products or fluid inclusions (Fig. 5c). The initial heating steps of a plagioclase grain from a third sample (site 2) are marked by the release of an excess argon component, likely associated with degassing of fluid inclusions as indicated by the high Cl/K ratios for these steps. The rest of the release spectrum is a well-behaved staircase spectrum with nearly $>50\%$ of radiogenic argon released in the final steps, in spite of the small wattage increments. The weighted average ages of the last five plagioclase heating steps are 1190 ± 2 and 1211 ± 3 Ma, in reasonable agreement with the ca. 1.2 Ga ages recorded by igneous biotite (Fig. 5).

Argon dating was also undertaken on a whole

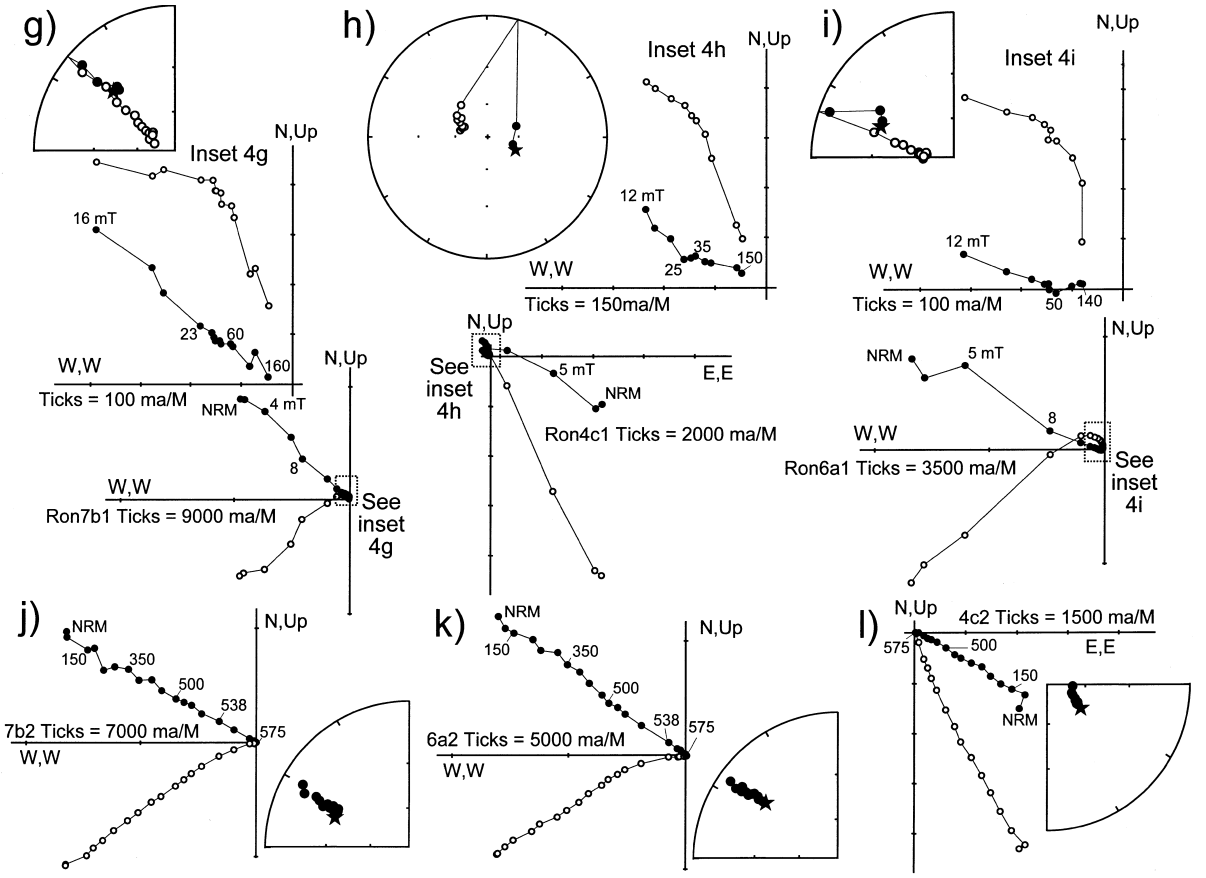

rock sample of the basalt (site 14), in spite of clear indications of hydrothermal alteration in thin section. A total gas age of 1062 ± 3 Ma is obtained from the whole rock sample, similar to the previously reported age 982 ± 10 Ma and 1038 ± 14 Ma for the basalts of the NFF [25]. The argon release spectrum for the whole rock sample shows a clear correlation between composition (both Ca/K and Cl/K ratios) and the inferred ages for the individual steps (Fig. 5d). Contributions from at least three phases can be discerned sequentially in the spectrum: an old phase poor in Cl and Ca, a young phase with an intermediate Ca and Cl content, and a Ca-rich, Cl-rich phase of intermediate age. Clearly, the geological significance of this whole rock spectrum is uncertain and only a minimum age can be assigned to the basalt from whole rock dating alone.

5. Discussion

Given the overwhelming contribution of magnetite to the observed fabric, we conclude that the magnetic lineations and foliations reflect an average magnetite grain shape. We conclude that the late-crystallizing magnetite grains were formed on a silicate 'template', as has been suggested by other authors [34]. The observed orientation of magnetic ellipsoids are consistent with a sill origin for the NFF gabbro with magnetic lineations possibly reflecting magmatic flow directions from a central vent. Significant to the paleomagnetic interpretation is the fact that this sill is undeformed and that no tilt correction is necessary. Petrographic observations reveal the igneous origin of the silicate and oxide mineralogy, suggesting that no subsequent metamorphism has affected the body.

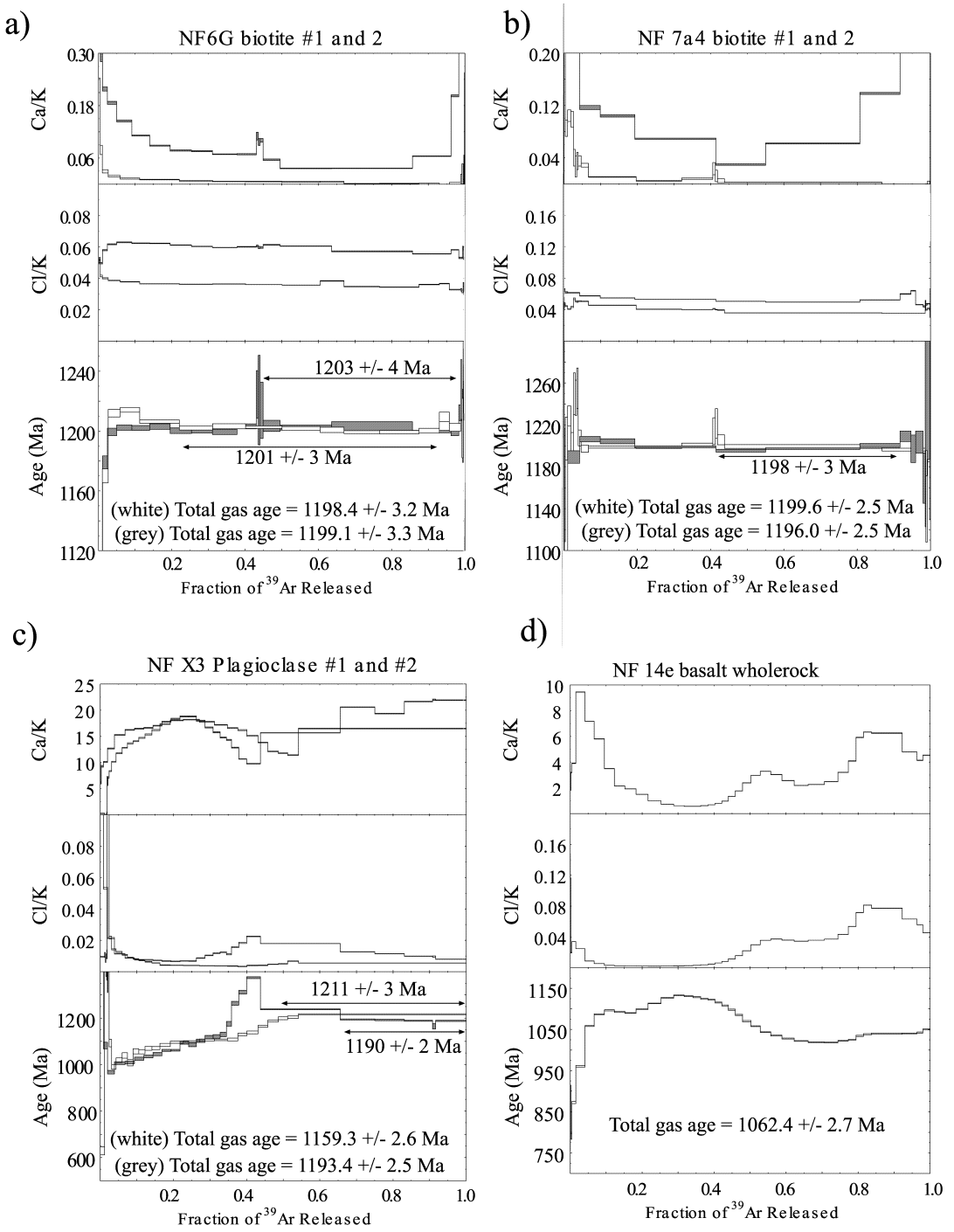

Fig. 5. Argon degassing spectra for two samples of igneous biotite (a, b); a plagioclase grain (c); and a whole rock basalt sample (d). Arrows on age spectra indicate the individual steps used to calculate plateau ages for each replicate.

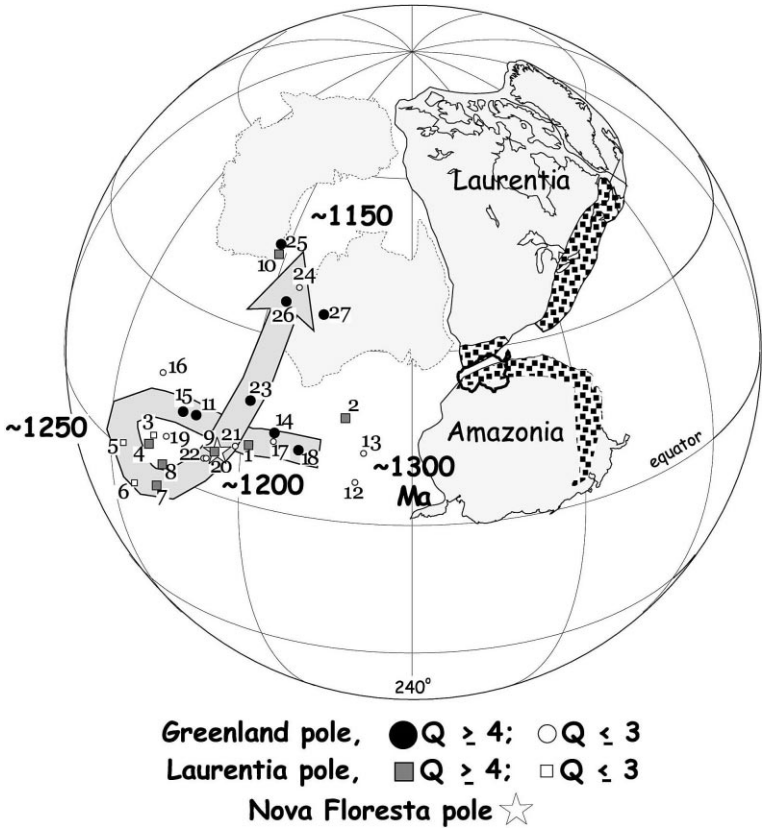

Fig. 6. Position of the Amazon craton according to Nova Floresta pole shown in modern Laurentia coordinates using the Euler pole [8.7, 280.2, −156.5]. The present-day northern margin of the Amazon craton is facing south in this figure as indicated by the isthmus of Panama. Note the proximity of the southwestern margin of the present day Amazon craton with the deformed Llano portion of the Laurentian margin. The position of the ca. 1.2 Ga Nova Floresta pole is shown with respect to the combined Laurentia/Greenland APWP for 1.3–1.15 Ga. Australia is depicted for reference in both the SWEAT [2] and the AUSWUS [46] configurations.

This is confirmed by the concordance of biotite and plagioclase ages, which we interpret as recording fast cooling following the emplacement of the magma. Thus, the pole calculated for the NFF ($n = 16$ sites, $P_{lat.} = 24.6°N$, $P_{long.} = 164.6°E$, $A_{95} = 5.5°$) is considered to be primary and in situ with a quality factor, Q, of 5 [35].

5.1. The 1.3–1.15 Ga APWP for Laurentia/Greenland

The overall shape of the Proterozoic APWP for Laurentia for 1300–1150 Ma has undergone substantial revision since early summary works [36,37] as geochronological results were refined and erroneous paleomagnetic results recognized. One important modification to these early proposed paths is the shortening of the 1.25–1.0 Ga Logan Loop [38,39]. The equatorial starting point of this loop is anchored by the well-dated, well-determined Mackenzie (1267 Ma) and Sudbury (1235 Ma) poles. Recent re-evaluations of the few data that defined the rounded, ascending limb of the loop (ca. 1.25–1.15 Ga) demonstrate that these are (i) poorly dated poles based on multiple dike generations, (ii) poles based on remagnetizations, or (iii) poles displaced due to improper structural correction [39–41]. Circumventing these poles results in a 'skinny' loop whose ascending limb at 1250 to 1150 is defined by a

Table 2
Selected paleomagnetic poles for Laurentia and Greenland from the 1.3–1.15 Ga interval

		Age constraints (Ma)[a]	A_{95}	$P_{lat.}$ (°N)	$P_{long.}$ (°E)	Age assigned	1	2	3	4	5	6	7	**Q**	Ref.
Laurentia:															
1	Nain Anorthosite	U_{zir} 1305 ± 15	3	11	211	1305	1	1	0	0	0	1	1	**4**	[48,49]
2	Harp Dykes	U_{bad} 1273 ± 1	7	19	228	1273	1	0	1	1	0	0	1	**4**	[50,51]
3	Muskox Int.	U_{bad} 1270 ± 4	6	6	191	1270	1	1	0	0	0	0	1	**3**	[52,53]
4	Mackenzie dikes	U_{bad} 1267 ± 2	5	4	190	1267	1	1	1	0	1	?	1	**5**	[53,54]
5	Copper Mine R.	1050–1300	6	1	183	1260	0	1	0	0	1	0	1	**3**	[52]
6	Savage Pt./Aston Bay Sills[b]	675–1240	11	−5	186	1240	0	1	0	0	1	0	1	**3**	[55]
7	Sudbury Dykes	U_{bad} $1235^{+7}/_{-3}$	3	−3	192	1235	1	1	1	1	1	0	1	**6**	[56,57]
8	Lower Bylot[c]	1174–1240	6	2	194	1220	1	1	0	0	1	0	1	**4**	[58–60]
9	Upper Bylot	Pb_{cal} 1204 ± 22	4	8	205	1200	1	1	0	0	1	1	1	**5**	[58–60]
10	Abitibi Dikes	U_{bad} 1141 ± 1	14	43	208	1141	1	1	1	1	1	0	1	**6**	[40,61,62]
Greenland[d]:															
11	Motzfeldt Int.	U_{ap} 1350 ± 23	12	10	212	1350	1	1	1	0	0	1	1	**5**	[44,63]
12	ZigZag Basalts		4	12	243	1300	0	1	0	0	1	0	1	**3**	[64]
13	Midsommersø Dolerite	Rb_{wr} ~1250	5	7	242	1300	0	1	0	0	0	0	1	**2**	[64]
14	Gronendal–Ika complex[e]	Rb_{wr} 1299 ± 17	8	12	227	1299	1	1	1	0	0	0	1	**4**	[65,66]
15	North Qoroq Intrusive	Rb_{wr} 1291 ± 62	12	13	203	1291	0	1	1	0	0	1	1	**4**	[44,66]
16	Nassarssuaq Stock	1230–1316	14	9	209	1291	0	0	1	0	0	0	1	**2**	[44]
17	BD0 dikes[f]	U 1280	14	11	227	1280	1	1	0	?	0	0	1	**3**	[45,67]
18	Victoria Fjord Dykes		6	10	232	1275	0	1	1	1	0	0	1	**4**	[68]
19	West Gardar Lamprophyre	Rb_{bio} 1254–1276	10	3	206	1265	1	0	0	0	0	0	1	**2**	[69]
20	West Gardar dikes (BD1)	1160–1316	10	3	215	1230	0	1	1	?	0	0	1	**3**	[45]
21	Gronedal district dikes	1160–1316	8	7	220	1228	0	0	1	?	0	0	1	**2**	[45]
22	Kimberlite (LK1)	Rb_{wr} 1227 ± 12	5	3	215	1227	1	0	0	0	0	0	1	**2**	[70]
23	Eriksfjord Lower[g]	Sm ~1185 ± 30	11	16	220	1185	1	1	1	0	1	0	1	**5**	[63,71,72]
24	Tugtutoq NNE dikes	U_{bad} 1163 ± 2	5	36	224	1163	1	0	0	0	0	0	1	**2**	[64,73]
25	South Qoroq Intrusive	Rb_{wr} 1160 ± 8	12	42	216	1160	1	1	1	0	0	1	1	**5**	[44,66]
26	West Gardar SW–NE dikes	1143–1154	5	34	222	1150	1	1	1	?	0	0	1	**4**	[45]
27	NE-SW dikes (BD2–BD3)	1143–1154	5	33	231	1149	1	1	1	?	0	0	1	**4**	[44]

[a] Age constraints from geological relations as reported by author or from direct radiogenic dating. Symbols for radiogenic system employed as follows: U_{zir} (U–Pb zircon); U_{bad} (U–Pb badelleyite); Pb_{cal} (Pb–Pb carbonate); U_{ap} (U–Pb apatite); Rb_{wr} (Rb–Sr whole rock isochron); Rb_{bio} (Rb–Sr biotite); and Sm (Sm–Nd plagioclase–pyroxene isochron). 1, age of rock unit known to within 40 Ma; 2, adequate no. of samples; 3, well-documented demagnetization; 4, field test; 5, structural control (note, continuity with craton is assumed here); 6, presence of reversals; 7, does not resemble younger pole.

[b] Combined pole calculated from [55].

[c] Combined from Nauyat Fm. and Adams Fm. as reported in [58].

[d] Greenland poles rotated to Laurentian coordinates using the Euler pole ($P_{lat.}$ 67.5°, $P_{long.}$ −118.5°, −13.8°) from [43].

[e] Grand mean recalculated from combined host rock amphibolites and intrusives sites reported in [65].

[f] Age data reported as preliminary.

[g] Grand mean recalculated from combined sites of [71,72].

more direct, NNE-oriented path (Fig. 6, squares). The return path during the Keweenawan interval is well-documented and has been discussed elsewhere [42].

Consideration of paleomagnetic results from Greenland, corrected for the opening of the Labrador Sea in the Tertiary [43], expands the list of available poles, especially for the 1300–1275 Ma interval for which Laurentian results are scarce. The majority of these paleomagnetic results come from the Gardar Province of SW Greenland, where three episodes of rifting and associated volcanism at ca. 1300–1280 Ma, ca. 1220 Ma, and ca. 1160–1125 Ma are preserved [44,45]. Although many of the Gardar dates are based on K–Ar and Rb–Sr data, we note that several anchor points for the combined APWP are provided by well-dated poles from Laurentia. In compiling the Laurentia/Greenland APWP, we have applied modern criteria for the evaluation of the reliability of a paleomagnetic result [35]. Specifically, we have excluded data from bodies with ambiguously documented paleomagnetic directions, and poles based on secondary magnetic overprints where identified by the original authors. In general, the selected Greenland poles confirm the inferred shape and polarity of the skeletal Laurentian APWP for the 1.25–1.15 Ga interval (Fig. 6, circles). Significantly, several poles from Greenland confirm the shortened, meridional version of the Logan Loop (cf. the Gardar track of Piper [44]). The NNE drift from the sub-equatorial Sudbury dikes pole position defines a small loop which crosses the earlier latitudinal path of 1300–1250 Ma (Table 2).

5.2. Paleogeography of the Amazon Craton

We use the ca. 1.2 Ga Nova Floresta pole as a constraint on the orientation and latitude of the Amazon craton. Comparing the attitude of Amazonia with that of Laurentia in the latter's northward drift from ~1.25 to 1.15 Ga permits the geographic proximity of these two cratons in an orientation that aligns the margins of both continents. We note that only the southernmost portion of Laurentia, i.e. the Llano segment, is at the same latitude as that portion of the western Amazon craton where early Grenville (inferred from hornblende $^{40}Ar/^{39}Ar$ cooling ages) deformation is observed. Furthermore, this juxtaposition of the western Amazon craton with the Llano portion of the Laurentian margin provides a test for the position of the ~1.2 Ga Nova Floresta pole with respect to the combined Laurentia/Greenland APWP. We consider the overlap of the NF pole with the 1.2 Ga segment of the Laurentia/Greenland APWP as strong evidence of Amazonia's possible role in the Llano collisional event (Fig. 6).

The ~1.2 Ga collision proposed here marks an early phase in the assembly of Rodinia along the Grenville margin. However, it is difficult to compare the Amazon–Laurentia collision within the framework of existing Rodinia reconstructions that depict the supercontinent at ~1.0 Ga, the generally accepted age for the final amalgamation [1,2,6,7]. By locating Amazonia at the southernmost portion of Laurentia's Grenville margin (modern coordinates), we establish a starting configuration for the ongoing assembly of Rodinia. We also note that the Amazon craton's position at the southern margin of Laurentia (Fig. 6) serves as a check on the position of continents that may have bordered Laurentia's southwestern margin in the SWEAT and AUSWUS reconstructions, but only for times of ~1.2 Ga [2,46].

5.3. The Llano Uplift

As stated previously, the Llano portion of the Laurentian Grenville belt was unmatched by a colliding continent in recent reconstructions [8,9]. If our proposed connection between western Brazil and the southernmost Grenville province of Laurentia is correct, the tectonic history of the Llano Uplift of west-central Texas should reflect this collision [11–13,47]. Preservation of mafic eclogites records an early, high P–T metamorphic event that is synchronous with early deformation. Timing of this high P–T event is constrained by the dating of metamorphic zircons that range in age from 1128 ± 6 to 1147 ± 4 Ma [47]. An additional younger constraint on the timing of deformation is provided by the youngest syntectonic granite intrusions, dated at 1119 ± 6 Ma [13]. These age constraints are in agreement with the

previously cited limits of 1238 ± 8 to 1098 ± 3 Ma [12]. However, as noted by Mosher [11], ages determined from syntectonic metamorphic minerals are unlikely to record the true age of deformation. Since metamorphic minerals typically record cooling from peak *T*-conditions, which post-date peak *P*-conditions in the clockwise *P–T* loop expected for continent–continent collision, these 'syntectonic' ages are likely to be younger than the true deformation age. Thus, we consider the age of the Amazon–Laurentia collision to be bracketed between about 1.24 and 1.12 Ga. A post-tectonic episode of granite emplacement resulted in regional, static metamorphism at low *P–T* amphibolitic conditions, resulting in widespread resetting of $^{40}Ar/^{39}Ar$ and Rb–Sr systems at 1098–1014 Ma [13].

Acknowledgements

The authors would like to thank Rommel da Silva Sousa for technical support with special thanks to Janio Amorim for field support from the CPRM office in Porto Velho, Rondônia. We thank Marcus Johnson and Chris Hall for assistance at the University of Michigan argon chronology laboratory and Eric Essene for many fruitful discussions of oxide petrology. Joe Meert and Ted Irving provided thoughtful reviews and helpful suggestions. We express thanks to Josep Pares and Arlo Weil for discussions of paleomagnetic techniques and Proterozoic tectonics. E. Tohver received funding from the Scott Turner Fund at the University of Michigan and a GSA Student Grant to complete field work. Research was funded by NSF grants EAR-96-14407 and EAR 99-80459. Additional funding was received from the Stichting Dr. Schurmannfonds (2001/11).*[AC]*

References

[1] P.F. Hoffman, Did the breakout of Laurentia turn Gondwana inside out?, Science 252 (1991) 1409–1412.
[2] I.W.D. Dalziel, Pacific margins of Laurentia and East Antarctica-Australia as a conjugate rift pair: evidence and implications for an Eocambrian supercontinent, Geology 19 (1991) 598–601.
[3] G.C. Bond, P.A. Nickeson, M.A. Kominz, Breakup of a supercontinent between 625 Ma and 555 Ma; new evidence and implications for continental histories, Earth Planet. Sci. Lett. 70 (1984) 325–345.
[4] P.A. Cawood, P.J.A. McCausland, G.R. Dunning, Opening Iapetus: constraints from the Laurentian margin in Newfoundland, Geol. Soc. Am. Bull. 113 (2001) 443–453.
[5] R. Trompette, Geology of Western Gondwana (2000–500 Ma): Pan-African-Brasiliano Aggregation of South America and Africa, Balkema Publishers, Rotterdam, 1994.
[6] A.B. Weil, R. Van der Voo, C. Mac-Niocaill, J.G. Meert, The Proterozoic supercontinent Rodinia; paleomagnetically derived reconstruction for 1100 to 800 Ma, Earth Planet. Sci. Lett. 154 (1998) 13–24.
[7] M.S. D'Agrello-Filho, R.I.F. Trinidade, R. Siqueira, C.F. Ponte-Neto, I.I.G. Pacca, Paleomagnetic constraints on the Rodinia supercontinent: implications for its Neoproterozoic break-up and the formation of Gondwana, Inter. Geol. Rev. 40 (1998) 171–188.
[8] I.W.D. Dalziel, S. Mosher, L.M. Gahagan, Laurentia–Kalahari collision and the assembly of Rodinia, J. Geol. 108 (2000) 499–513.
[9] C.M. Powell, D.L. Jones, S. Pisarevsky, M.T.D. Wingate, Paleomagnetic constraints on the position of the Kalahari craton in Rodinia, Precambrian Res. 110 (2001) 33–46.
[10] A. Davidson, An overview of Grenville Province geology, Canadian shield, in: S.B. Lucas, M.R. St. Onge, Geology of the Precambrian Superior and Grenville Provinces and Precambrian Fossils in North America, Chap. 3, Geol. Surv. Can. 7, 1998, pp. 205–270.
[11] S. Mosher, Tectonic evolution of the southern Laurentian Grenville orogenic belt, Geol Soc. Am. Bull. 110 (1998) 1357–1375.
[12] N. Walker, Middle Proterozoic geologic evolution of Llano uplift, Texas: evidence from U–Pb zircon geochronometry, Geol. Soc. Am. Bull. 104 (1992) 494–504.
[13] J.R. Rougvie, W.D. Carlson, P. Copeland, J.N. Connelly, Late thermal evolution of Proterozoic rocks in the northeastern Llano Uplift, central Texas, Precambrian Res. 94 (1999) 49–72.
[14] S. Hanmer, Ductile thrusting at mid-crustal level, southwestern Grenville Province, J. Can. Earth Sci. 25 (1988) 1049–1059.
[15] S.J. McEachern, O. Van Breemen, Age of deformation within the Central Mestasedimentary Belt boundary thrust zone, southwest Grenville Orogen: constraints on the collision of the Mid-Proterozoic Elzevir terrane, Can. J. Earth Sci. 30 (1993) 1155–1165.
[16] J. McLelland, J.S. Daly, J.M. McLelland, The Grenville Orogenic Cycle (ca. 1350–1000 Ma) an Adirondack perspective, Tectonophysics 265 (1996) 1–28.
[17] S. Hanmer, D. Corrigan, S. Pehrsson, L. Nadeau, SW Grenville Province, Canada the case against post 1.4 Ga accretionary tectonics, Tectonophysics 319 (2000) 33–51.
[18] K. Mezger, B.A. van der Pluijm, E.J. Essene, A.N. Halli-

day, Synorogenic collapse a perspective from the middle crust, the Proterozoic Grenville Orogen, Science 254 (1991) 695–698.
[19] T. Rivers, J. Martignole, C.F. Gowers, A. Davidson, New tectonic divisions of the Grenville Province, Southeast Canadian Shield, Tectonics 8 (1989) 63–84.
[20] T.E. Krogh, Precise U–Pb ages for Grenvillian and pre-Grenvillian thrusting of Proterozoic and Archean metamorphic assemblages in the Grenville Front Tectonic Zone, Canada, Tectonics 13 (1994) 963–982.
[21] H.A. Wasteneys, S.L. Kamo, D. Moser, T.E. Krogh, C.F. Gower, J.V. Owen, U–Pb geochronological constraints on the geological evolution of the Pinware terrane and adjacent areas, Grenville Province, southern Labrador, Canada, Precambrian Res. 81 (1997) 101–128.
[22] J.E. Scandolâra, G.J. Rizzotto, J.L. de Amorim, R.B.C. Bahia, M.L. Quadros, C.R. da Silva, Geological map of Rondônia 1:1000 000, Companhia de Pesquisa de Recursos Minerais, Rio de Janeiro, 1999.
[23] E. Tohver, B.A. van der Pluijm, J.E. Scandolâra, M.C. Geraldes, Rodinia and the Amazonia–Laurentia connection: preliminary *D–P–T–t* results in western Brazil, Abstr. Prog. Geol. Soc. Am. 32 (2000) 385.
[24] M. Litherland, R.N. Annells, D.P.F. Darbyshire, C.J.N. Fletcher, M.P. Hawkins, B.A. Klinck, W.I. Mitchell, E.A. O'Connor, P.E.J. Pitfield, G. Power, B.C. Webb, The Proterozoic of eastern Bolivia and its relationship to the Andean mobile belt, Precambrian Res. 43 (1989) 157–174.
[25] J.W.L. Leal, G.H. Silva, D.B. dos Santos, W. Teixeira, M.I.C. de Lima, C.A.C. Fernandes, A. Pinto, Folha SC. 20, Porto Velho, (Monograph) Projeto RADAMBRASIL, vol. 16, Departamento Nacional de Producao Mineral, Rio de Janeiro, 1978, pp. 17–184.
[26] S.J. Romanini, Geologia e resultados prospectivos das areas Serra dos Pacaás Novos e Rio Cautário, Rondônia, Companhia de Pesquisa de Recursos Minerais, Porto Allegre, 2000.
[27] J.S. Bettencourt, R.M. Tosdal, W.B. Leite, B.L. Payolla, Mesoproterozoic rapakivi granites of the Rondônia Tin Province, southwestern border of the Amazonian craton, Brazil. I. Reconnaissance U–Pb geochronology and regional implications, Precambrian Res. 95 (1999) 41–67.
[28] V. Jelinek, Characterization of the magnetic fabric of rocks, Tectonophysics 79 (1981) 63–67.
[29] J.L. Kirschvink, The least-squares line and plane and the analysis of paleomagnetic data, Geophys. J. R. Astron. Soc. 62 (1980) 699–718.
[30] J.D.A. Zijderveld, AC demagnetization of rocks: analysis of results, in: D.W. Collison, S.K. Runcorn, K.M. Creer (Eds.), Methods in Paleomagnetism, Elsevier, New York, 1967, pp. 254–286.
[31] J.C. Roddick, High precision intercalibration of $^{40}Ar/^{39}Ar$ standards, Geochim. Cosmochim. Acta 47 (1983) 887–898.
[32] S.E. Haggerty, Oxidation of opaque mineral oxides in basalts, Reviews in Mineralogy, Min. Soc. Am. 3, 1976, pp. Hg1–100.
[33] D.H. Tarling, F. Hrouda, The Magnetic Anisotropy of Rocks, Chapman and Hall, New York, 1993.
[34] R.B. Hargraves, D. Johnson, C.Y. Chan, Distribution anisotropy: the cause of AMS in igneous rocks, Geophys. Res. Lett. 12 (1991) 2193–2196.
[35] R. Van der Voo, The reliability of paleomagnetic data, Tectonophysics 184 (1990) 1–9.
[36] E. Irving, J.C. McGlynn, Proterozoic magnetostratigraphy and the tectonic evolution of Laurentia, Philos. Trans. R. Soc. Lond. A 280 (1976) 433–468.
[37] J.L. Roy, Paleomagnetism of the North American Precambrian: a look at the database, Precambrian Res. 19 (1983) 319–348.
[38] W.A. Robertson, W.F. Fahrig, The Great Logan Paleomagnetic Loop: the polar wandering path from Canadian Shield rocks during the Neohelikian Era, Can. J. Earth Sci. 8 (1971) 1355–1372.
[39] H.C. Palmer, H.C. Halls, Paleomagnetism of the Powder Mill Group, Michigan and Wisconsin a reassessment of the Logan Loop, J. Geophys. Res. 91 (1986) 11,571–11,580.
[40] R.E. Ernst, K.L. Buchan, Paleomagnetism of the Abitibi dyke swarm, southern Superior Province and implications for the Logan Loop, Can. J. Earth Sci. 30 (1993) 1886–1897.
[41] K.L. Buchan, S. Mertanen, R.G. Park, L.J. Pesonen, S.Å. Elming, N. Abrahamsen, G. Bylund, Comparing the drift of Laurentia and Baltica in the Proterozoic: the importance of key paleomagnetic poles, Tectonophysics 319 (2000) 167–198.
[42] H.C. Halls, L.J. Pesonen, Paleomagnetism of Keweenawan rocks, Geol. Soc. Am. Mem. 156 (1982) 173–201.
[43] W.R. Roest, S.P. Srivastava, Sea-floor spreading in the Labrador Sea a new reconstruction, Geology 17 (1989) 719–722.
[44] J.D.A. Piper, The paleomagnetism of major (Middle Proterozoic) igneous complexes, South Greenland and the Gardar apparent polar wander track, Precambrian Res. 54 (1992) 153–172.
[45] J.D.A. Piper, The paleomagnetism of middle Proterozoic dyke swarms of the Gardar Province and Mesozoic dykes in SW Greenland, Geophys. J. Int. 120 (1995) 339–355.
[46] K.E. Karlstrom, K.I. Åhäll, S.S. Harlan, M.L. Williams, J. McLelland, J.W. Geissman, Long-lived (1.8–1.0 Ga) convergent ororgen in southern Laurentia, its extensions to Australia and Baltica, and implications for refining Rodinia, Precambrian Res. 111 (2001) 5–30.
[47] R.C. Roback, Characterization and tectonic evolution of a Mesoproterozoic island arc in the southern Grenville Orogen, Llano Uplift, central Texas, Tectonophysics 265 (1996) 29–52.
[48] G.S. Murthy, Paleomagnetic results from the Nain anorthosite and their tectonic implications, Can. J. Earth Sci. 15 (1978) 516–525.
[49] R.F. Emslie, W.D. Loveridge, Fluorite-bearing early and middle Proterozoic granites, Okak Bay area, Labrador;

geochronology, geochemistry and petrogenesis, Lithos 28 (1992) 87–109.
[50] E. Irving, R.F. Emslie, J.K. Park, Paleomagnetism of the Harp Lake Complex and associated rocks, Can. J. Earth Sci. 14 (1977) 1187–1201.
[51] A.C. Cadman, J. Tarney, W.R.A. Baragar, R.J. Wardle, Relationship between Proterozoic dykes and associated volcanic sequences-evidence from the Harp swarm and Seal Lake Group, Labrador, Canada, Precambrian Res. 68 (1994) 357–374.
[52] W.R.A. Baragar, W.A. Robertson, Fault rotation of paleomagnetic directions in Coppermine River Lavas and their revised pole, Can. J. Earth Sci. 10 (1973) 1519–1532.
[53] A.N. LeCheminant, L.H. Heaman, Mackenzie igneous events, Canada: Middle Proterozoic hotspot magmatism associated with ocean opening, Earth Planet. Sci. Lett. 96 (1989) 38–48.
[54] E. Irving, J.K. Park, J.C. McGlynn, Paleomagnetism of Et-Then Group and Mackenzie diabase in Great Slave Lake area, Can. J. Earth Sci. 9 (1972) 744–767.
[55] D.L. Jones, W.F. Fahrig, Paleomagnetism and age of the Aston dykes and Savage Point sills of the Boothia Uplift, Canada, Can. J. Earth Sci. 15 (1978) 1605–1612.
[56] E.J. Schwarz, K.L. Buchan, Uplift deduced from remanent magnetization; Sudbury area since 1250 Ma ago, Earth Planet. Sci. Lett. 58 (1982) 65–74.
[57] F.O. Dudas, A. Davidson, K.M. Bethune, Age of the Sudbury diabase dykes and their metamorphism in the Grenville Province, Ontario. Radiogenic age and isotopic studies, Report 8, Geol. Sur. Can., Curr. Res. 1994F, 1994, pp. 97–106.
[58] W.F. Fahrig, K.W. Christie, D.L. Jones, Paleomagnetism of the Bylot basins; evidence for Mackenzie continental tensional tectonics, Geol. Sur. of Canada, Paper 81–10, 1981, pp. 303–312.
[59] G.D. Jackson, T.R. Ianelli, B.J. Tilley, Rift-related sedimentation and volcanism on northern Baffin and Bylot Islands, District of Franklin, in: Curr. Res. Part I, Geol. Surv. of Can. Paper 80-10, 319–328.
[60] L.C. Kah, T.W. Lyons, J.T. Chesley, Geochemistry of a 1.2 Ga carbonate-evaporate succession, northern Baffin and Bylot Islands: implications for Mesoproterozoic marine evolution, Precambrian Res. 111 (2001) 203–234.
[61] T.E. Krogh, F. Corfu, D.W. Davis, G.R. Dunning, L.M. Heaman, S.L. Kamo, N. Machado, J.D. Greenough, E. Nakamura, Precise U–Pb isotopic ages of diabase dykes and mafic to ultramafic rocks using trace amounts of baddeleyite and zircon, in: H.C. Halls, W.F. Fahrig (Eds.), Mafic Dyke Swarms, Geol. Assoc. Can. Spec. Paper 34, 1987, pp. 147–152.
[62] E. Irving, A.J. Naldrett, Paleomagnetism in Abitibi greenstone belt, and Abitibi and Matachewan diabase dikes; evidence of the Archean geomagnetic field, J. Geol. 85 (1977) 157–176.
[63] C.R. Paslick, A.N. Halliday, G.R. Davies, K. Mezger, B.G.J. Upton, Timing of Proterozoic magmatism in the Gardar Province, southern Greenland, Geol. Soc. Am. Bull. 105 (1993) 272–278.
[64] C. Marcussen, N. Abrahamsen, Paleomagnetism of the Proterozoic Zig-Zag Dal Basalt and the Midsommersø Dolerites, eastern North Greenland, Geophys. J. R. Astron. Soc. 73 (1983) 367–387.
[65] J.D.A. Piper, Paleomagnetism of the Mesoproterozoic Grønnedal-Íka alkaline complex, Southwest Greenland, Precambrian Res. 69 (1994) 51–60.
[66] A.B. Blaxland, O. van Breemen, C.H. Emeleus, J.G. Anderson, Age and origin of the major syenite centers in the Gardar province of South Greenland: Rb–Sr studies, Geol. Soc. Am. Bull. 89 (1978) 231–244.
[67] A.C. Cadman, L. Heaman, J. Tarney, R. Wardle, T.E. Krogh, U–Pb geochronology and geochemical variation within two Proterozoic mafic dyke swarms, Labrador, Can. J. Earth Sci. 30 (1993) 1490–1504.
[68] N. Abrahamsen, R. Van der Voo, Paleomagnetism of middle Proterozoic (ca. 1.25 Ga) dykes from central North Greenland, Geophys. J. R. Astron. Soc. 91 (1987) 597–611.
[69] J.D.A. Piper, J.E.F. Stearn, Paleomagnetism of the dyke swarms of the Gardar Igneous Province, South Greenland, Phys. Earth Planet. Int. 14 (1977) 345–358.
[70] J.D.A. Piper, Paleomagnetic study of the (Late Precambrian) West Greenland kimberlite-lamprophyre suite: definition of the Hadrynian Track, Phys. Earth Planet. Int. 27 (1981) 164–186.
[71] D.N. Thomas, J.D.A. Piper, A revised magnetostratigraphy for the Mid-Proterozoic Gardar lava succession, South Greenland, Tectonophysics 201 (1992) 1–16.
[72] J.D.A. Piper, Magnetic stratigraphy and magnetic-petrologic properties of Precambrian Gardar lavas, South Greenland, Earth Planet. Sci. Lett. 34 (1977) 247–263.
[73] K.L. Buchan, R.E. Ernst, M.A. Hamilton, S. Mertanen, L. Pesonen, S.Å. Elming, Rodinia: the evidence from integrated paleomagnetism and U–Pb geochronology, Precambrian Res. 110 (2001) 9–32.